

Spring 2015

Doppler Shifted Internal Waves in a Shallow Water Region

William D. Boll
Old Dominion University

Follow this and additional works at: https://digitalcommons.odu.edu/oeas_etds



Part of the [Oceanography Commons](#)

Recommended Citation

Boll, William D.. "Doppler Shifted Internal Waves in a Shallow Water Region" (2015). Master of Science (MS), Thesis, Ocean & Earth Sciences, Old Dominion University, DOI: 10.25777/c26d-hr43
https://digitalcommons.odu.edu/oeas_etds/330

This Thesis is brought to you for free and open access by the Ocean & Earth Sciences at ODU Digital Commons. It has been accepted for inclusion in OES Theses and Dissertations by an authorized administrator of ODU Digital Commons. For more information, please contact digitalcommons@odu.edu.

**DOPPLER SHIFTED INTERNAL WAVES IN A
SHALLOW WATER REGION**

by

William D. Boll
B.S. May 2009, Georgia Institute of Technology


A Thesis Submitted to the Faculty of
Old Dominion University in Partial Fulfillment of the
Requirements for the Degree of

MASTER OF SCIENCE


OCEAN AND EARTH SCIENCES

OLD DOMINION UNIVERSITY
May 2015

Approved by:



Chester E. Grosch (Director)



Tal Ezer (Member)



John M. Klinck (Member)

ABSTRACT

DOPPLER SHIFTED INTERNAL WAVES IN A SHALLOW WATER REGION

William D. Boll
Old Dominion University, 2015
Director: Dr. Chester E. Grosch

Measurements of velocity fields from a high frequency (1.2 MHz) vertical acoustic doppler current profiler (VADCP) along with density and temperature profiles were taken in coastal waters on the New Jersey shelf. Time series span six consecutive months from May through October 2003, capturing the transition of the water column from a highly stratified summer into a fully mixed winter season. Barotropic tides interact with variations in local bathymetry causing disturbances within the fluid medium which govern internal wave characteristics. During the months of June, July, and August, a high number of internal wave signals were observed. Spectra from depth averaged vertical velocities have a relatively constant structure for frequencies greater than 36 h^{-1} until reaching the cut-off frequency of 90 h^{-1} . Wave periods ranged from 40 s to 15 min with variability mostly due to fluctuations in regional dynamics. Evidence supports propagating internal waves in the direction of the bathymetric gradient towards shore. Wavelet analysis of depth averaged vertical signals reveal an alteration in frequency that has a period comparable to the tidal cycle. Peaks in frequencies were observed near high tide before decreasing back to a lower value. More than 70 of these instances occurred during the data collection period. Evidence supports Doppler shifted internal waves by the horizontal moving tide. The observation of this unique phenomenon provided motivation for this study. The scope of this work analyzes one such occurrence in detail followed by the inspection of values averaged over the month of August. Analysis

techniques include evaluating water column properties, correlations between instrumentation, along with the examination of theoretical models.

ACKNOWLEDGMENTS

Thanks to Dr. Ann E. Gargett. Her interests have led to the collection of this data set for which she has graciously allowed me to use in my studies. I would greatly like to commend my advisor, Dr. Chet E. Grosch. Without his patience and guidance I surely would have gone astray. I also want to thank my committee members Dr. Tal Ezer and Dr. John M. Klinck and the support from the Department of Ocean, Earth & Atmospheric Sciences and the Center for Coastal Physical Oceanography at Old Dominion University.

I want to largely acknowledge my parents, Greg and Paula Boll, for their encouragement and support in all of my endeavors. My sister September, for whose strength I admire. Lastly, I am utterly grateful for my compassionate wife, Kristen Anstead, for who I dearly love.

TABLE OF CONTENTS

	Page
LIST OF TABLES.....	viii
LIST OF FIGURES	ix
INTRODUCTION	1
INSTRUMENTATION	5
LOCAL AND REGIONAL DYNAMICS.....	9
STRATIFICATION.....	9
SPECTRA	13
TIDES	15
CORRELATIONS	18
EVENT ANALYSIS.....	21
DISCUSSION.....	30
CONCLUSIONS.....	35
REFERENCES	36
APPENDIX.....	39
VITA	42

LIST OF TABLES

Table	Page
1. Monthly averaged maximum buoyancy values and their standard deviation.....	14
2. Dominant tidal periods and their attributes as predicted by T_TIDE.....	15
3. Monthly observed events and number of high tides measured by the VADCP.	33

LIST OF FIGURES

Figure	Page
1. Location of Node B and local bathymetry.....	5
2. Instrumentation setup at LEO-15's Node B (39.46°N, 74.24°W).....	6
3. Sample vertical velocity record for 14 July, 2003.....	7
4. Geometry of instrument locations at Node B	8
5. Available data collected by the VADCP, CTD profiler, thermistor string and the meteorological tower.....	8
6. Monthly averaged salinity profiles for 2003.....	10
7. Monthly averaged density, left, and buoyancy, right, profiles	11
8. Maximum buoyancy frequencies calculated from available CTD data.....	11
9. Monthly averaged wind speeds and their standard deviation from the mean.....	12
10. Sample wind stress and direction for 21-22 July, 2003	12
11. Horizontal current magnitudes for 21-22 July, 2003	12
12. Monthly power spectra of the vertical component of velocity	14
13. Depth averaged temperature profiles for August 2003.....	16
14. Power spectra of depth averaged temperature profiles for August, 2003	16
15. Tidal amplitudes for the month of August, 2003 as predicted by T_TIDE using 35 constituents	17
16. Tidal ellipses from horizontal velocities as predicted by TOPEX for six tidal cycles beginning on 25 August, 2003 using constituents from Table 1	18
17. Bathymetry transect from Fig. 1 along the flood vector.....	18
18. Correlations and p-values between vertical velocity amplitude and tidal amplitude for high tide on 26 August at 10:57	20

Figure	Page
19. Lag plot, top, and minimum correlation values, bottom, from all correlations between depth averaged vertical velocity and tidal amplitude	20
20. Wind stress, top, and direction, bottom, for 26 August, 2003	21
21. Averaged density, left panel, and buoyancy, right, profiles for 26 August, 2003	22
22. Vertical velocity time series, top, and the wavelet, bottom for 26 August, 2003	23
23. First five modes for two-layer numerical internal wave model	25
24. Dynamic calculation of modal speeds for the first five modes	25
25. Depth averaged horizontal magnitude along the flood vector	26
26. Correlations for the $\omega = 3.85 \text{ h}^{-1}$ frequency between the VADCP and thermistor string	27
27. Froude number values for 26 August, 2003	27
28. Reconstructed observed vertical oscillation frequency overlaid on vertical frequency wavelet for 26 August, 2003	29
29. Vertical oscillation frequencies, top, and horizontal speeds along the flood vector and Froude values, bottom, for the month of August, 2003	32
30. Density and buoyancy profiles for 13:24, 26 August, 2003	34

INTRODUCTION

The regular flow of tides over bathymetry is an effective generator of internal waves. Lines of constant density within the stratified water column become forced in the vertical direction, producing restoring oscillations that uniquely characterize the propagating wave (Bell 1975). Barotropic tides moving over stationary bathymetric features generate some of the most energetic waves within the interior of the ocean (Baines 1982; Hibiya 1986; Munk and Wunsch 1998). This input of energy is then cascaded at various scales through numerous wave processes, generating turbulence, and ultimately dissipating as heat (Richardson 1926). Tides themselves undergo a significant energy loss during the production of baroclinic internal tides and lose about 0.4 TW globally to this process (Baines 1982; Egbert and Ray 2001, 2003; Llewellyn Smith and Young 2002).

In general, an internal wave is the response of a fluid due to some disturbance occurring within the stably stratified medium. Buoyancy and gravity are the natural vertically restoring forces of a statically stable environment and can be characterized by the Brunt-Väisälä stability frequency (Gill 1982; Phillips 1966):

$$N^2 = -\frac{g}{\rho_o} \frac{\partial \rho(z)}{\partial z}. \quad (1)$$

Here, g is the gravitational constant, ρ_o is the reference density of the fluid and the differential quotient is the density gradient with respect to depth. A measure of stratification is the buoyancy frequency given in Eq. (1). Internal waves satisfy a dispersion relation and their angular frequency is limited by the coriolis frequency, f , and the stability frequency:

$$f \leq \omega \leq N, \quad (2)$$

where ω is the wave's angular frequency. A sharp drop in energy exists within the global spectrum for internal waves near this upper limit (Gould 1971; Cairns 1974). Once frequencies exceed this constraint the wave decays rapidly as a local patch of turbulent fluctuations (Cushman-Roisin and Beckers 2007).

For waves generated at the continental shelf near New Jersey, the sloping bottom acts as a wave guide directing them upslope in a northwest direction, parallel to the bathymetric gradient (Kunze et al. 2002; Hallock and Field 2005). Overall, any type of flow over a stationary feature is capable of producing disturbances within the stratified medium.

Research shows that when the ratio of the angle of propagation of an internal wave to the slope in bathymetry is unity, turbulence is likely (Legg and Adcroft 2003; Ezer et al. 2011). The critical parameter is given as:

$$\alpha = \frac{s}{((\omega^2 - f^2)/(N^2 - \omega^2))^{1/2}}, \quad (3)$$

where s is the slope of the sea floor and the denominator is the angle of the propagating internal wave in terms of its angular frequency ω , coriolis frequency f , and buoyancy frequency N .

Understanding the local flow regime is important when examining internal waves propagating within a non-stationary medium. Flow regimes within a fluid is based on the established theory of supercritical flows and the criterion used is the non-dimensional Froude number (Legg and Adcroft 2003);

$$F = \frac{U}{c_p}, \quad (4)$$

and is a function of the horizontal speed, U , and the phase speed, c_p , of the wave. When the speed of the wave exceeds the speed of the fluid, $F < 1$, subcritical flow is present and information propagates upstream (Hibiya 1986). The wave will propagate downstream in the case of a supercritical regime, $F > 1$. When $F = 1$, critical flow exists and resonance occurs, resulting in the storing of energy in the form of a standing wave. Internal wave breaking is possible when the Froude number reaches some maximum value, allowing for dissipation to take place in the form of turbulence (Legg 2014). Solitons are highly nonlinear internal waves that can result from a regime shift near bathymetric features or river plumes (Apel et al. 1997). Typically, frequencies of propagating solitons appear in rank order with the lowest frequencies observed first, followed by increasingly higher frequencies. The phenomenon under investigation in this study appears to be solitons initially; however, depth averaged vertical speeds exhibit a decrease in frequency after a maximum is observed.

A Doppler shift is the observed change in frequency emitted from a moving source relative to a stationary location. The natural frequency of a stationary source is perceived as increased when the source approaches an observer (blue shifted). When the source is moving away from the observer, the measured frequency is decreased (red shifted). The equation used to describe the observed change in frequency is:

$$\omega(t)_{obs} = \omega_{true} \frac{1}{(1 - F)}. \quad (5)$$

Here, F is the Froude number from Equation 4, ω_{obs} is the observed frequency while ω_{true} is the natural frequency of a stationary source.

Internal waves are observed to propagate on the Northeast coast of the United States and on the New Jersey shelf. A periodic change in frequency measured from the vertical velocity occurs and is comparable in time to one tidal cycle. The concept of Doppler shifted frequencies is applied in this study to internal waves propagating within moving ocean currents under changing regimes. Instrumentation and location of this study's focus will be discussed in Section II followed by a description of the local dynamics on the New Jersey shelf and the Middle Atlantic Bight, including spectra and tidal characteristics, in Section III. A single event is then analyzed in detail under nearly ideal conditions in Section IV. A discussion with an explanation of the observations is given in in Section V followed by concluding remarks in Section VI.

INSTRUMENTATION

A five-beam vertical acoustic doppler current profiler (VADCP) was deployed roughly 7 km off shore on the New Jersey shelf at LEO-15's Node B cabled oceanic observatory platform located near 39.46°N, 74.24°W (Fig. 1) (Gargett and Wells 2007; Tejada-Martinez and Grosch 2007). The VADCP is a broadband instrument that

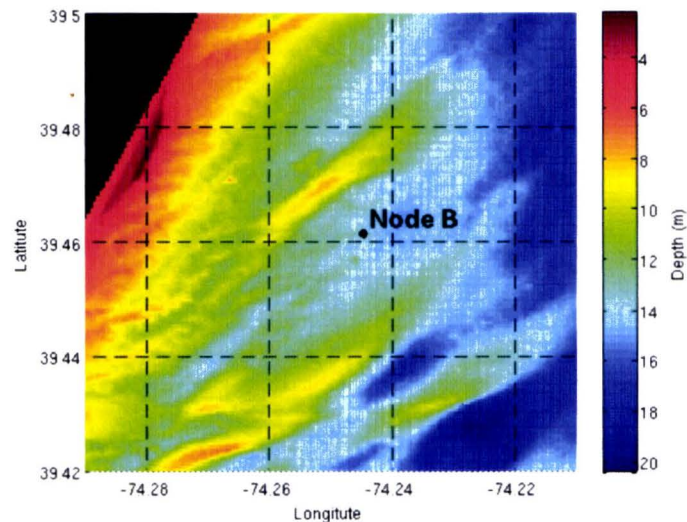


FIG. 1. Location of Node B and local bathymetry. The bathymetry data was obtained from the National Oceanic and Atmospheric Administration (NOAA) National Geophysical Data Center (NGDC) and was surveyed from 23 October, 2003 – 25 January, 2004 under project number OPR-C303-KR-03 (H11241).

incorporates four standard slant beams each directed 30° from the vertical, along with a fifth transducer directed upwards which allows the vertical velocity in the column to be measured directly. The device was held in place atop a securely anchored platform 4 cm above the sandy bottom which was attached to a 2 m long post driven into the clay bed beneath (Fig. 2). The Mid-Atlantic Bight National Undersea Research Center supplied power to Node B and all instrumentation during the study period. Operating at a 1.2 MHz broadband frequency, the VADCP resolves the entire 15 m water column. Horizontal

velocities are derived from appropriate slant beams and are calculated relative to the instrument configuration and then transformed into a geographical coordinate system.

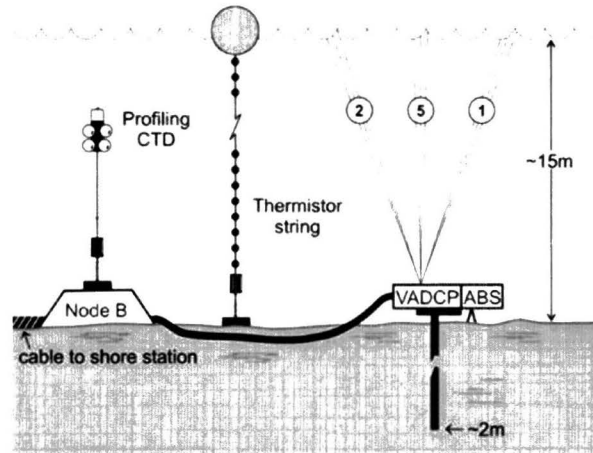


FIG. 2. Instrumentation setup at LEO-15's Node B (39.46°N , 74.24°W).

Measurements were taken roughly every second creating a time series that spans over six consecutive months, capturing the transition from summer into the winter season. Horizontal and vertical velocities of the water column are displayed as profiled time series in 40 cm incremental bins. The VADCP data stream was broken into sessions containing multiple records, each of length ~ 2.3 hours for processing purposes by the original investigators. Record lengths are roughly one fifth of the dominant semi-diurnal tidal period at LEO-15. Vertical velocity profiles of a sample record for 14 July, 2003 displayed a relatively high amplitude vertical speed compared to background velocities (Fig. 3). The observed wave train demonstrates initially high amplitudes that encompass the majority of the water column followed by decreasing amplitudes and vertical extent over the 2 h time period.

The cabled observatory contains a profiling CTD which operates on an irregular schedule with multiple profiles obtained daily. In-situ temperature, salinity and pressure measurements were obtained during each collection period. Additional temperature

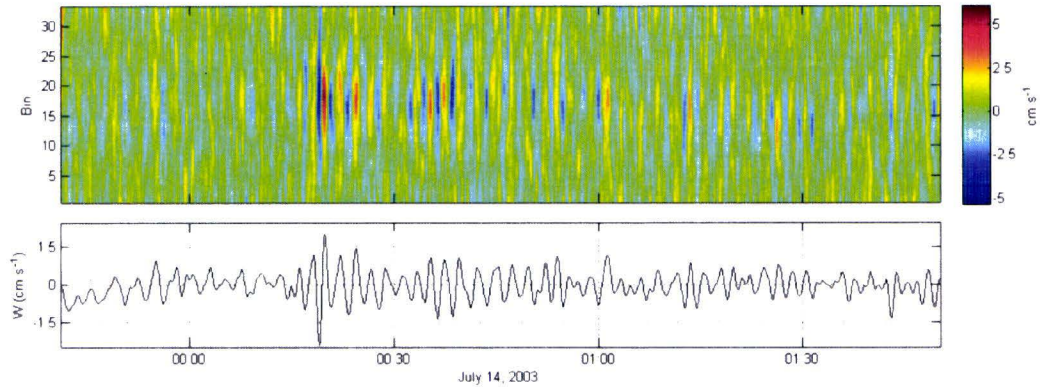


FIG. 3. Sample vertical velocity record for 14 July, 2003. VADCP data, top, and depth averaged velocities, bottom. The horizontal axis is hours.

profiles were acquired from a thermistor string that spans the depth of the water column located 105 m southeast from Node B (Fig. 4). Thermistors were equally spaced every 25 cm and took readings of instantaneous temperatures every four minutes. Meteorological data includes wind speed and direction obtained every minute from the Rutgers University Field Station located onshore in Tuckerton, New Jersey at 39.51°N, 74.32°W. Available data for each instrument varied over the six month collection period (Fig. 5).

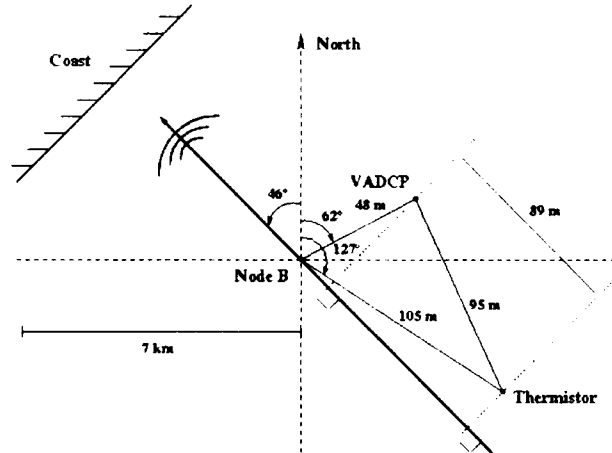


FIG. 4. Geometry of instrument locations at Node B. The VADCP is located 48 m from Node B with a bearing of 62° from north and the thermistor string is located 105 m from Node B with a bearing of 127° from north. The tidal flood vector is indicated by the thick solid black arrow with wave crests.

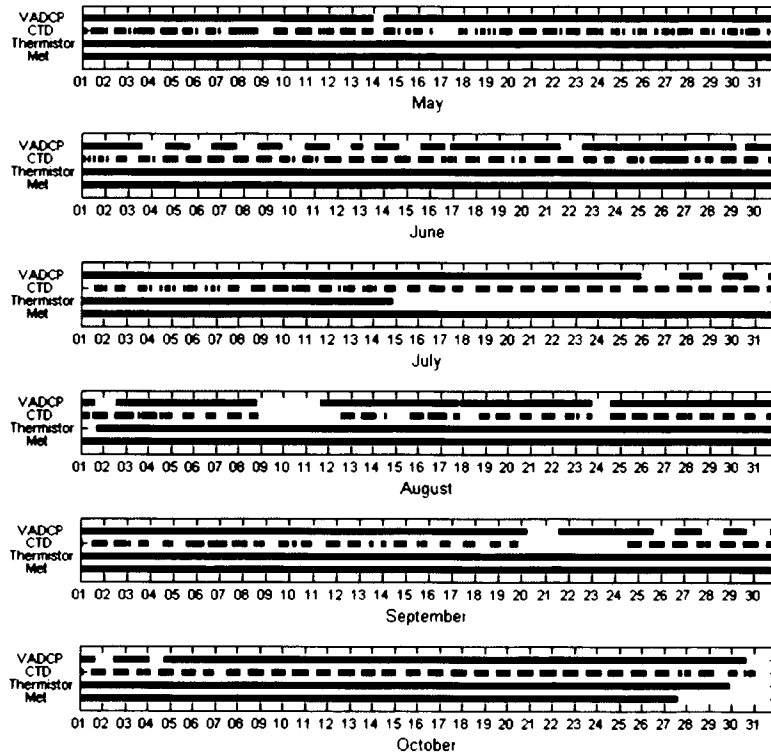


FIG. 5. Available data collected by the VADCP, CTD profiler, thermistor string and the meteorological tower. Solid lines indicate collected data. The horizontal axis is days.

LOCAL AND REGIONAL DYNAMICS

STRATIFICATION

The Middle Atlantic Bight (MAB) is the Northeast area of the U.S. continental shelf that extends southward 800 km from Cape Cod, Massachusetts to Cape Hatteras, North Carolina. The shelf is gently sloped and has a typical width of 100 km. Mean current dynamics on the MAB have been studied extensively and are generally directed along-shelf (Bumpus 1973; Beardsley et al. 1976; Beardsley and Boicourt 1981). The southwest flowing coastal boundary current is derived from the Labrador Current which is mostly cold water originating from the Arctic Ocean and glacial melt from the Greenland ice sheet (Chapman and Beardsley 1989). Just off the shelf in deeper waters is the much larger scale Gulf Stream that flows in an opposing northeast direction (Beardsley and Winant 1979). During summer seasons a large source of less dense freshwater is supplied to the coastal boundary current by several rivers that are predominantly comprised of the Hudson River outflow. This freshwater mass takes about 40 days to reach the southern coast of New Jersey (Yankovski and Garvine 1998). Monthly averaged salinity profiles show that the month of June possessed the largest gradient from surface to bottom in 2003 (Fig. 6).

Shallow water regions of the MAB are characterized during the summer as being intensely stratified. Density profiles taken from the profiling CTD at Node B showed signs of instability, signifying that mixing has taken place. More dense water overtop lower densities indicate overturning. To obtain real values of buoyancy, density structures were reordered appropriately to represent ideally stable water column profiles (Thorpe 2007). Computing buoyancy profiles was accomplished using the 2010

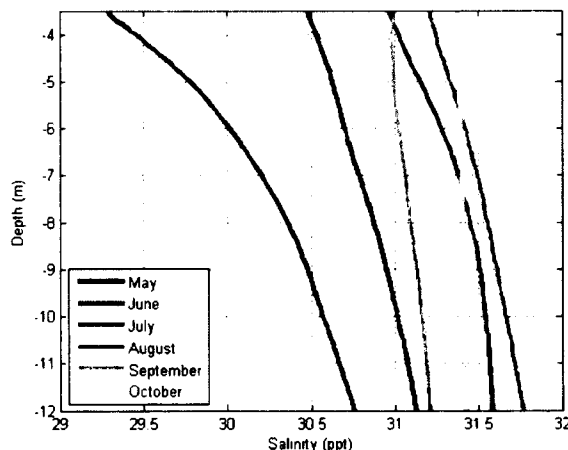


FIG. 6. Monthly averaged salinity profiles for 2003.

Gibbs-SeaWater Oceanographic Toolbox (McDougall and Barker 2011). Increased stratification is present during the months of June, July and August (Fig. 7). A sharp decrease in maximum buoyancy frequencies from individual profiles occurred after the beginning of September (Fig. 8) and agrees well with month averaged profiles. Winter storms with longer durations and greater intensities during this transition period are responsible for vertically homogenizing the water column.

Variability of horizontal mean currents is found to be highly correlated with winds during the summer seasons due to the existence of a strong pycnocline. Summer winds are generally weaker than those in the fall and influence only the upper portion of the water column. In the winter, the column becomes well mixed with nearly uniform density and is heavily affected by flow over bathymetry (Kohut et al. 2004). Monthly averaged wind speeds and their deviation from the mean are increased for the months of September and October, 2003 near the coast of New Jersey (Fig. 9). A strong wind event during July is provided as an example to illustrate the effects of wind on the interior of the water column (Fig. 10). Wind stress calculations are based on Smith (1988). The

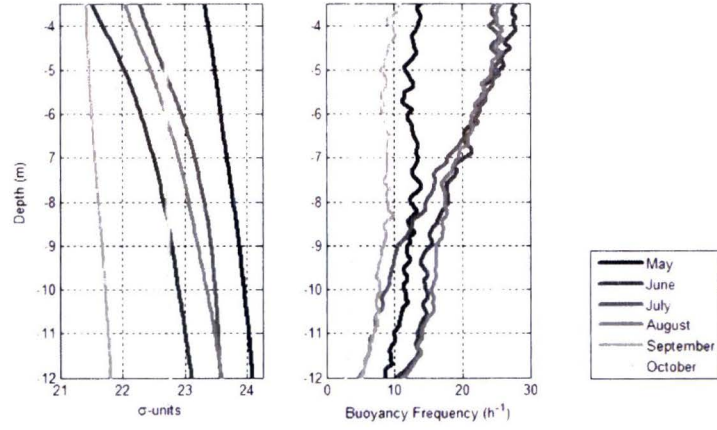


FIG. 7. Monthly averaged density, left, and buoyancy, right, profiles. The units of density are in sigma units: $\sigma = \rho_{S,T,p}[\text{kg m}^3] - 1000$.

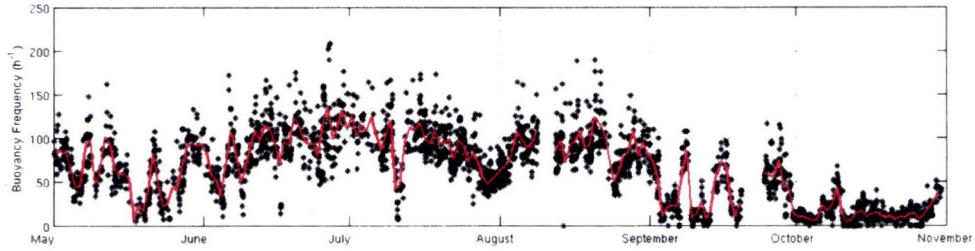


FIG. 8. Maximum buoyancy frequencies calculated from available CTD data.

average wind speed during this 18 h time period of 9.17 m s^{-1} is greater than one standard deviation from the monthly mean. In this example, winds blew in a constant direction over a sufficient time that allowed for the generation of a horizontal current near the surface. VADCP measurements indicate variations in the horizontal currents are located above the pycnocline in the upper two meters. The flow direction averaged over the time period is $38.9^\circ \pm 14.9^\circ$ east of the direction the wind is blowing towards, and falls within standard Ekman response criteria (Fig. 11).

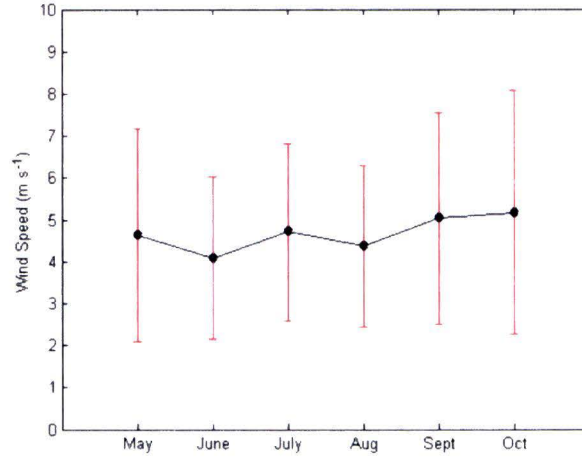


FIG. 9. Monthly averaged wind speeds and their standard deviation from the mean.

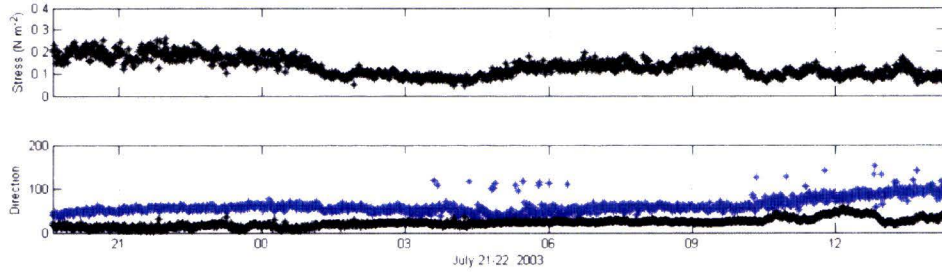


FIG. 10. Sample wind stress and direction for 21-22 July, 2003. Bottom panel: black asterisks are wind direction and blue asterisks are averaged top five surface bins of horizontal current. Angles are degrees clockwise from north and the horizontal axis is hours.

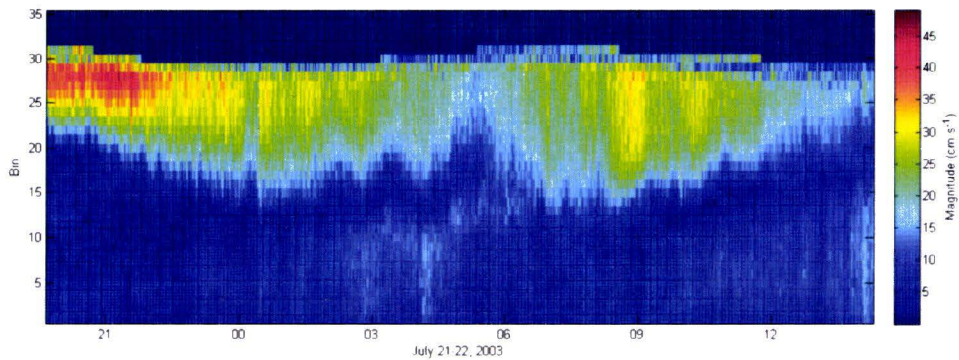


FIG. 11. Horizontal current magnitudes for 21-22 July, 2003. Horizontal axis is hours.

SPECTRA

Spectra of the vertical speed for all available VADCP data have been computed via the Fast Fourier Transform. Velocity magnitudes for each ping were averaged over the total number of bins in order to obtain a time series of vertically averaged vertical speed. During this process, data was interpolated at equally spaced intervals of one second for each 2.3 h record. Filtering and de-trending was not implemented during this initial stage of processing in order to preserve long term signals during the reconstruction of a time series consisting of multiple records.

A single time series of depth averaged vertical velocities was assembled for each month. A high pass fourth-order Butterworth filter with a cutoff frequency of 1 h^{-1} was used to remove tidal signals. The mean was subtracted and then the signal was normalized by its standard deviation. Finally a linear trend was removed followed by a second normalization before spectra were computed. In general, all spectra decrease in power from low to high frequencies with an apparent drop in power near 90 h^{-1} (Fig. 12). This is the natural cutoff frequency previously discussed in Section I. Variation of the cutoff frequency is due to the stratification, and waves with frequencies greater than this value decay rapidly. The monthly averaged maximum buoyancy values and their standard deviations from the mean are shown in Table 1 for each month. A relatively high buoyancy frequency is present for the months June - August. Averaged maximum buoyancy values for the months of September and October abruptly decrease and are the result of storms fully mixing the water column.

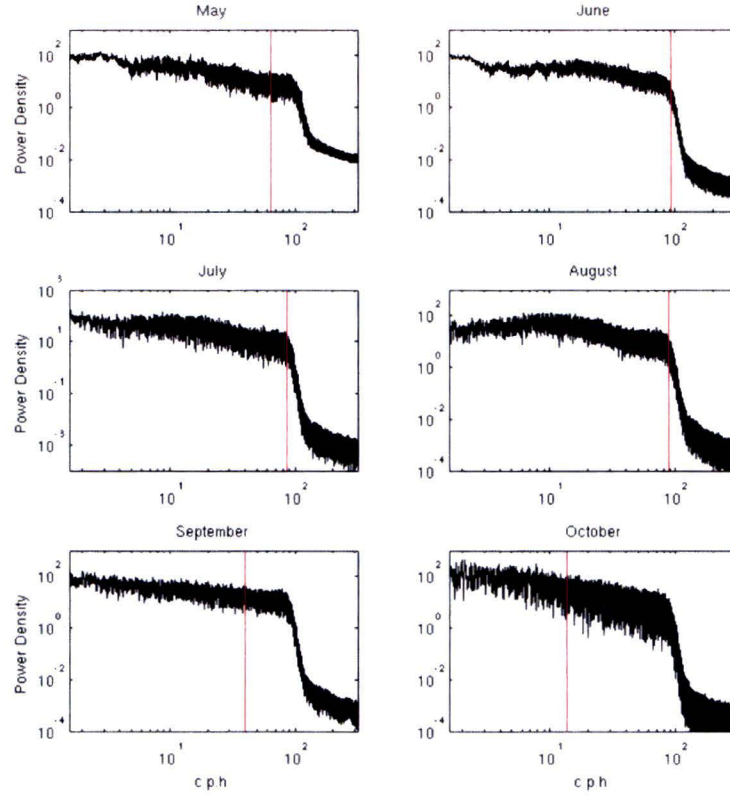


FIG. 12. Monthly power spectra of the vertical component of velocity. Axes are on log scales. Black lines are original spectra and vertical red lines are monthly averaged maximum buoyancy values.

TABLE. 1. Monthly averaged maximum buoyancy values and their standard deviation.

Month	$N_{MAX,AVG}$	STD
May	64.84 h^{-1}	16.55 h^{-1}
June	93.25 h^{-1}	15.32 h^{-1}
July	86.20 h^{-1}	31.52 h^{-1}
August	89.26 h^{-1}	28.87 h^{-1}
September	39.84 h^{-1}	22.68 h^{-1}
October	13.63 h^{-1}	22.36 h^{-1}

TIDES

Tidal height amplitudes were calculated from the Node B pressure sensor. The observed time series of water elevation is used to compute major tidal constituents from the tidal analysis toolbox T_TIDE (Pawlowicz et al. 2002). Predicted tides were estimated using roughly one million data points which span the entire six month duration. A total of 35 tidal constituents with 95% confidence were identified and their significance was determined by the ratio of signal to noise (major components are listed in Table 2).

TABLE. 2. Dominant tidal periods and their attributes as predicted by T_TIDE.

Tide	Description	Signal/Noise	Freq (h^{-1})	Period (h)	Amplitude (m)
M2	principal lunar	3.1e+3	0.0805	12.42	0.591
K1	luni-solar diurnal	2.8e+2	0.0418	23.93	0.112
N2	larger lunar elliptic	1.8e+2	0.0790	12.65	0.140
O1	principal lunar diurnal	1.2e+2	0.0387	25.81	0.0716
S2	principal solar	83	0.0833	12.00	0.109

Node B is characterized as having mixed tides dominated by the lunar M2 tidal constituent. Large tidal amplitudes occur every fortnight near spring tide. Maximum tidal amplitudes predicted for the month of August occur roughly twice every synodic month (Fig. 13). Vertical red lines are full and new moon phases, and indicated when tidal forces are the strongest (Espanak 2010). The product of high frequency filtered depth averaged temperature profiles for the month of August indicates multiple daily oscillations (Fig. 13). Power spectra of the resulting temperature time series were then computed (Fig. 14). Dominant periods are 12.37 h and 24.28 h which are the M2 and K1

tidal constituents. Tidal horizontal velocities are predicted from altimeter data and are used to construct tidal ellipses for six consecutive tidal cycles near new moon time on 27 August (Egbert and Erofeeva 2002). Modeled data provides a much cleaner indicator for maximum and minimum horizontal tidal velocities without interference from varying horizontal flow. The tidal vector rotates clockwise at Node B and the flood vector is calculated to be 46.06° counter-clockwise from north (Fig. 16). This vector is used as the

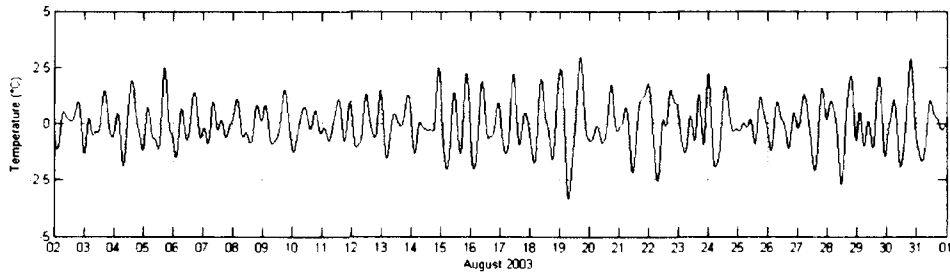


FIG. 13. Depth averaged temperature profiles for August 2003. Horizontal axis is days.

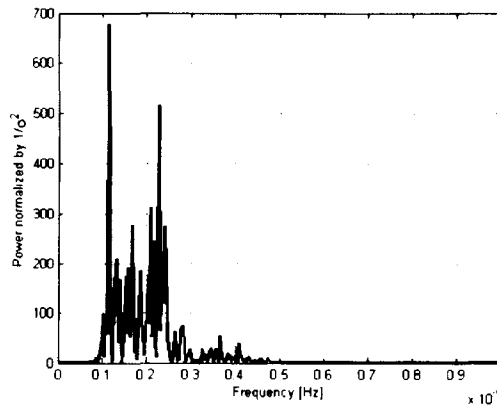


FIG. 14. Power spectra of depth averaged temperature profiles for August, 2003. Dominant periods are 24.28 h and 12.37 h.

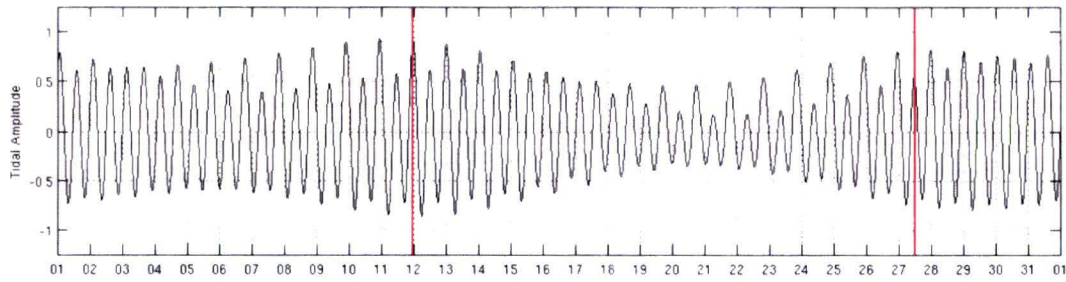


FIG. 15. Tidal amplitudes for the month of August, 2003 as predicted by T_TIDE using 35 constituents. Vertical red lines indicate maximum tidal forcing on full and new moon times. The horizontal axis are days of the month and the amplitude are in units of metres.

reference direction throughout this study. Here, and based on previous findings in the MAB region, the assumption is made that internal waves propagate in mostly the same direction as the flood vector and towards the coast. The distance between the VADCP and the thermistor string is 95.23 m and projecting their locations onto the flood vector reveals a corrected distance of 89.38 m (Fig. 4). Bathymetry along the flood vector over Node B had a linear fitted slope of 0.0598° (Fig. 17).

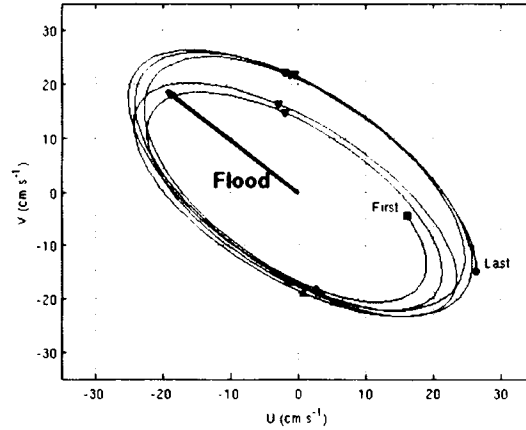


FIG. 16. Tidal ellipses from horizontal velocities as predicted by TOPEX for six tidal cycles beginning on 25 August, 2003 using constituents from Table 1. High and low tide occur where shaded triangles are pointing up and down, respectively.

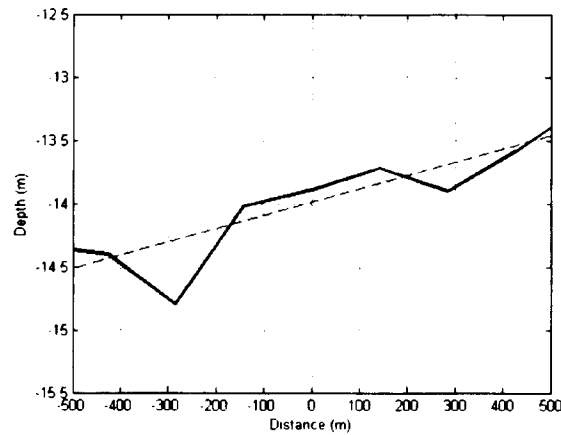


FIG. 17. Bathymetry transect from Fig. 1 along the flood vector. Horizontal axis is distance from Node B with values decreasing further from the coast.

CORRELATIONS

Correlations between vertical speed and tidal height amplitudes are calculated. Local high tide times were determined from the Node B pressure sensor and are used as a reference time for each correlation. To obtain a broad understanding of lag times, time series for both vertical velocity and tidal signals were assembled with lengths of ± 27 h

from high tide providing a total duration of 2.25 days; including four tidal cycles. Predicted tidal amplitudes from T_TIDE were used for the tidal series. Spearman's rank correlations were used in determining correlations. In all calculations, the tidal series was held fixed and the VADCP data series was shifted. The result is a series of correlation coefficients, along with their associated p-value, for a single pair of time series. P-values < 0.0001 are highly significant. With this approach, negative lag is interpreted as the tidal signal leading. Correlation coefficients and p-values for lags between velocity and tidal amplitudes were periodic and the time between averaged coefficient peaks is 12.62 h and is roughly the M2 tidal constituent (12.42). High tide occurring on 26 August, 2003 at 10:57 has a lag time of 2.01 h after maximum vertical velocity is observed (Fig. 18). The average lag time for all significant lags of dominant coefficients for each high tide over the six month study period is 2.56 h (Fig. 19). This difference in phase is the material response time, and given the standard deviation of $std = 0.73$ h, falls within the theoretical $\pi/2$ phase shift.

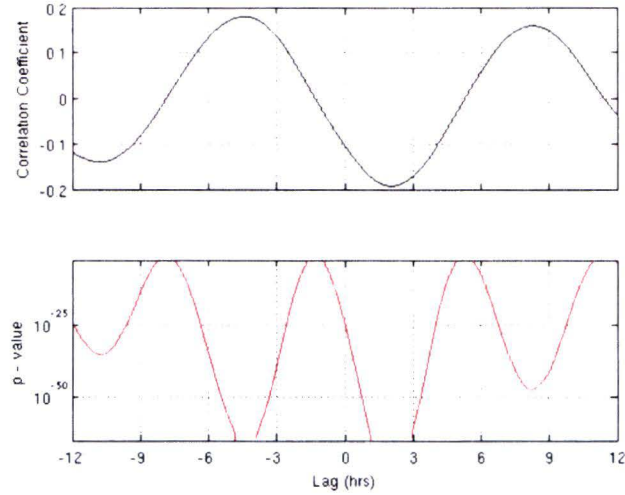


FIG. 18. Correlations and p-values between vertical velocity amplitude and tidal amplitude for high tide on 26 August at 10:57. The horizontal axis has been cropped to only display two tidal cycles.

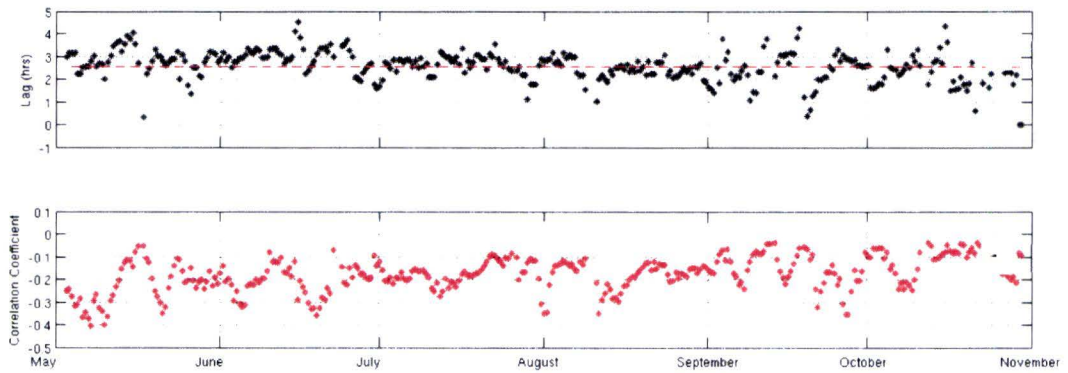


FIG. 19. Lag plot, top, and minimum correlation values, bottom, from all correlations between depth averaged vertical velocity and tidal amplitude. Dotted red line, top, is the average lag time of 2.56 h.

EVENT ANALYSIS

A single event is characterized in this study as an observed change in frequency of measured vertical oscillations occurring over a period of time that is comparable to the tidal cycle length. The observed change in frequency is cyclic with a maximum achieved near high tide. This section focuses on the analysis of a single event that took place on 26 August, 2003. Wind speeds during this event were low and average 2.84 m s^{-1} , and were one standard deviation below the average wind speed for August. Effects could only be identified in the two uppermost surface bins (80 cm). For comparison, wind stresses throughout this period are an order of magnitude lower than the example shown in Figure 10 from the previous section (Fig. 20).

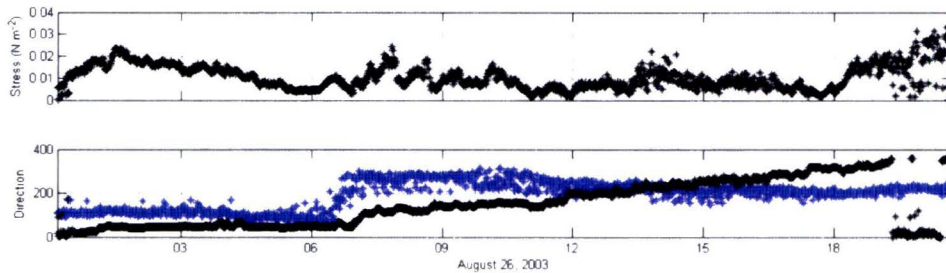


FIG. 20. Wind stress, top, and direction, bottom, for 26 August, 2003. Bottom panel: black asterisks are wind direction and blue asterisks are averaged top five surface bins of horizontal current. Angles are degrees clockwise from north and the horizontal axis is hours.

The water column, on average, remains continuously stratified with depth for the duration of this event. Averaged buoyancy profiles computed from eleven density profiles available on 26 August are within reason of the month's average (Fig. 21). Vertical overturning was apparent during the latter period of the event; the vertical extent

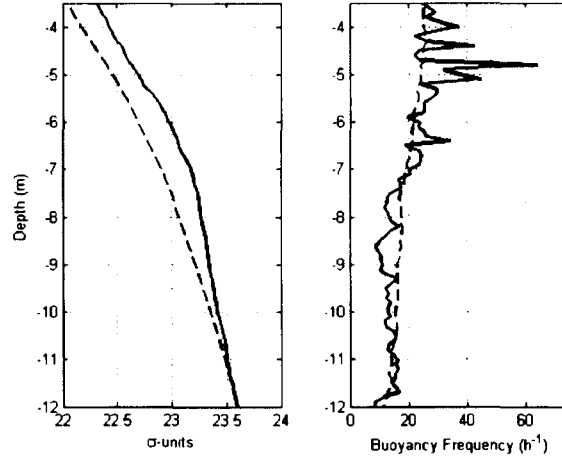


FIG. 21. Averaged density, left panel, and buoyancy, right, profiles for 26 August, 2003. Dashed lines are month averages. Densities are sigma units: $\sigma = \rho_{S,T,p}[\text{kg m}^3] - 1000$.

of mixing increased as the event progressed. Instabilities will be addressed in the discussion section of this manuscript

Wavelet analysis is a tool for analyzing localized variations in power within a time series and is used to observe the changes in frequency over time. A series decomposed into time-frequency space is created and dominant signals can be observed to evolve in time (Torrence and Compo 1998). Time series of the vertical velocity was constructed to encompass a period that is ± 13 h from the time when tidal amplitude is at a maximum. The series was then band-pass filtered, forward and backwards in time preserving the phase, with a fourth order Butterworth filter with cutoff frequencies of $1.33 \text{ h}^{-1} \leq \omega \leq 60 \text{ h}^{-1}$. The wavelet of the resulting time series displays color contours of dominant frequencies plotted over time with red and blue indicating high and low power, respectively (Fig. 22). The cone of influence, indicated by the near vertical solid black lines on the left and right, is also plotted in the bottom panel of this figure. Any signal

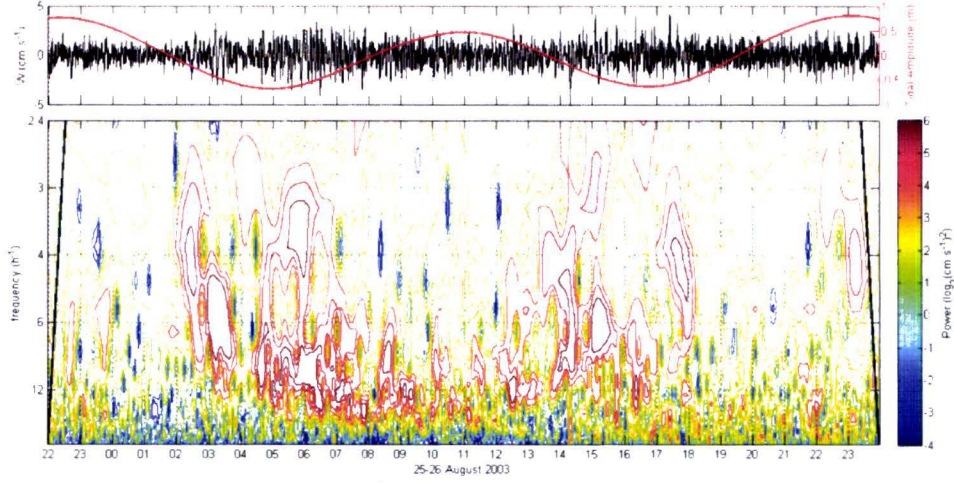


FIG. 22. Vertical velocity time series, top, and the wavelet, bottom for 26 August, 2003. Top: constructed depth averaged vertical velocity time series, black, and tidal amplitudes minus the mean sea surface height, red. Bottom: wavelet of the vertical velocity. Horizontal axis is hours.

inside the cone of influence is 95% significant while signals outside are not. A change in the dominant frequency is apparent. High power initially lies within lower frequencies beginning after hour 02 and then increase to a maximum frequency near the time of high tide. The change in measured dominant frequency is cyclical and decreases back to lower frequencies. The total period is comparable to the averaged tidal cycle (12.62 h).

The observed oscillations in the depth averaged vertical speed time series indicate the potential for internal waves. A numerical model was constructed in an effort to determine characteristics for propagating internal waves at the LEO-15's Node B site. Methods used to derive the model are discussed in the Appendix. Based on the averaged buoyancy profile for this event (Fig. 21), a two-layer model was considered appropriate. Averaged values of buoyancy and their associated depths are:

$$N(z) = \begin{cases} N_1 = 28.7 \text{ h}^{-1} & -h < z < 0 \\ N_2 = 13.7 \text{ h}^{-1} & -H < z < -h' \end{cases} \quad (6)$$

here, $h = 7$ m and $H = 15$ m. Phase speeds are calculated using (Phillips 1966):

$$c_p = \frac{\omega}{k}. \quad (7)$$

A dispersion diagram was constructed for the first five vertical modes by varying frequencies ω for wavenumbers k . A mode one internal wave has a maximum phase speed near 7.00 cm s^{-1} (Fig. 23). Dynamic calculations for long wave approximation modal speeds are in close agreement with the numerical model results (Fig. 24) (Gill 1982).

Rearranging Eq. (5) allows for the natural frequency to be obtained assuming the observed vertical signal is an altered frequency of a single mode internal wave. When the horizontal background speed has zero magnitude, the Froude value is negligible and the frequency can be found directly. Current speeds are the depth averaged horizontal speeds projected onto the flood direction (Fig. 26). A depth averaged horizontal speed of zero transpires between the hours 05 and 06 on 26 August. The dominant frequency of 3.85 h^{-1} occurs within that time period in the wavelet. Numerical model results for a propagating mode one internal wave indicates this frequency corresponds to a wavelength of 62.2 m with a phase speed equal to 6.77 cm s^{-1} . The projected distance between the VADCP and the thermistor string is 89.4 m. Given the phase speed, the mode one internal wave had a travel time of 22.0 min between the two instruments.

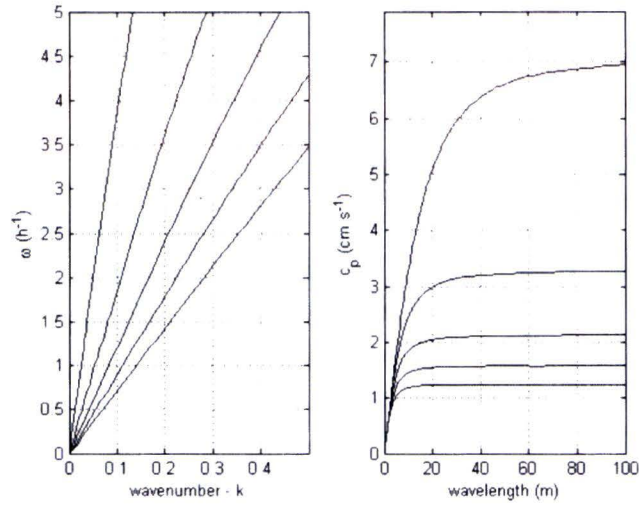


FIG. 23. First five modes for two-layer numerical internal wave model. Dispersion diagram, left, and corresponding phase speeds, right. $k = 2\pi/\lambda$ is the wavenumber.

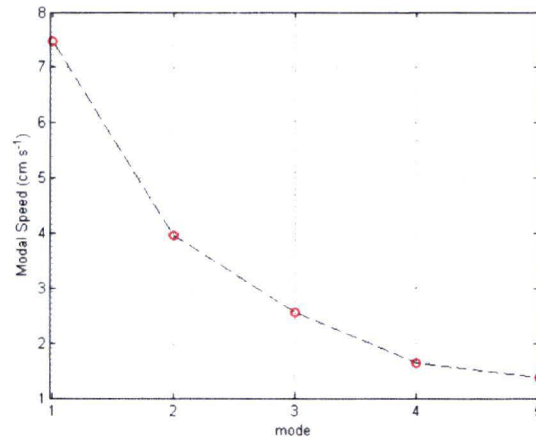


FIG. 24. Dynamic calculation of modal speeds for the first five modes.

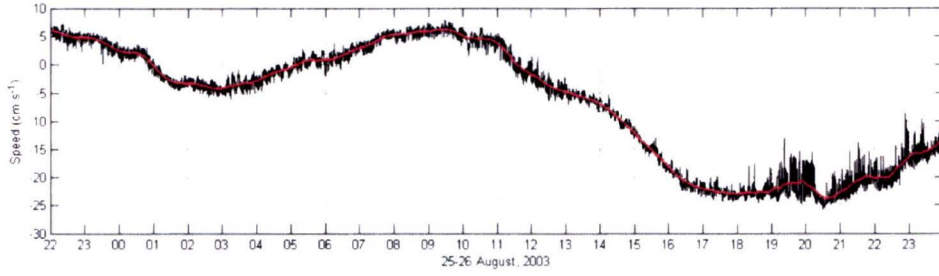


FIG. 25. Depth averaged horizontal magnitude along the flood vector. Red solid line is smoothed data. Horizontal axis is hours.

Wavelets from both the VADCP and the thermistor string provide arrival times for specific vertical oscillation frequencies at each location. Correlations between the two separate wavelets were calculated at the frequency $\omega = 3.85 \text{ h}^{-1}$ and were adjusted for a $\pi/2$ phase shift. A maximum correlation occurred at $-24 \pm 4 \text{ min}$ (Fig. 26). Negative lag indicates the signal travels from the thermistor string to the VADCP location, consistent with upslope propagation. The uncertainty is derived from the sampling rate of the thermistor string. This lag time is in agreement with the 22.0 min travel time for a mode one internal wave with phase speed 6.77 cm s^{-1} .

The flow regime is determined by calculating the non-dimensional Froude number from Eq. (4). Current speeds along the flood direction and the model output phase speed, $c_p = 6.77 \text{ cm s}^{-1}$ were used to construct a time series of corresponding Froude values. Dominant frequencies from wavelet analysis of depth averaged vertical speeds appeared after hour 02 and increase over roughly a six hour time period to hour 08. During this time the flow regime was subcritical and horizontal background flow was predominantly opposite of the flood direction. This indicates the wave is flowing upstream and towards the coast. Around hour 09, observed frequencies reached a

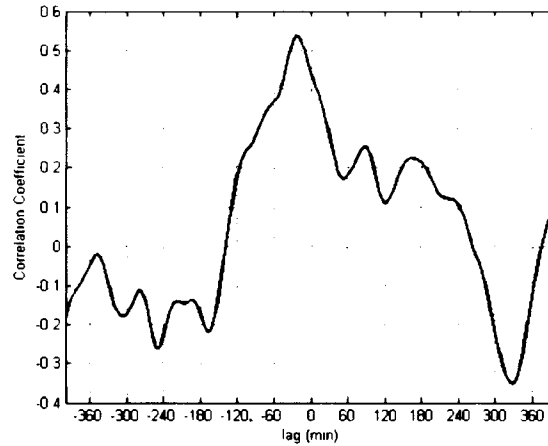


FIG. 26. Correlations for the $\omega = 3.85 \text{ h}^{-1}$ frequency between the VADCP and thermistor string.

maximum near 12 h^{-1} and the Froude number reached a critical value; resonance occurs between the wave and horizontal flow, and resulted in a standing wave. Over the next several hours (hours 10-13) the regime is subcritical and the wave continues to propagate towards the coast in the direction of the flood vector. Near the end of the event an intrusion of strong horizontal currents appeared and highly forced the flow regime to become highly supercritical. This had the effect of destroying the internal wave structure and generating a turbulent field.

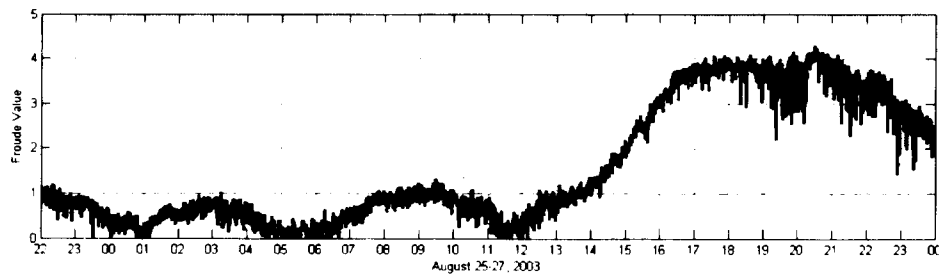


FIG. 27. Froude number values for 26 August, 2003. Critical flow is indicated by the horizontal dashed red line. Horizontal axis is hours.

Using the Doppler equation, the observed vertical oscillation frequencies can be reconstructed from the calculated Froude values. The results agree reasonably well during the increase in frequencies observed for the first half of the event (Fig. 28). Increases in frequencies occur and reach maximums close to the same time. Equation (5) does not fully support the observed changes in frequency for the time period after a maximum in frequencies were reached and a standing wave was present. Calculated frequencies decrease faster over a shorter period of time than what was observed. At this point, the density gradient of the water column became weaker due to vertical mixing. An intrusion of water mass has also altered the horizontal flow and increased the overall depth averaged speed in the direction opposite of the flood vector (Fig. 25). Equation 5 does not incorporate other phenomena that may take place within the medium of propagation and is intended for theoretical flow of a source emitting a fixed frequency.

Examining the relationship between local bathymetry and internal wave propagation angles, α remains less than 0.01 and subcritical, given an appropriate range of buoyancy values from this event (Eq. 3). The continental slope up the coast is indeed gentle and interactions of waves with the bottom would not result in a turbulent environment.

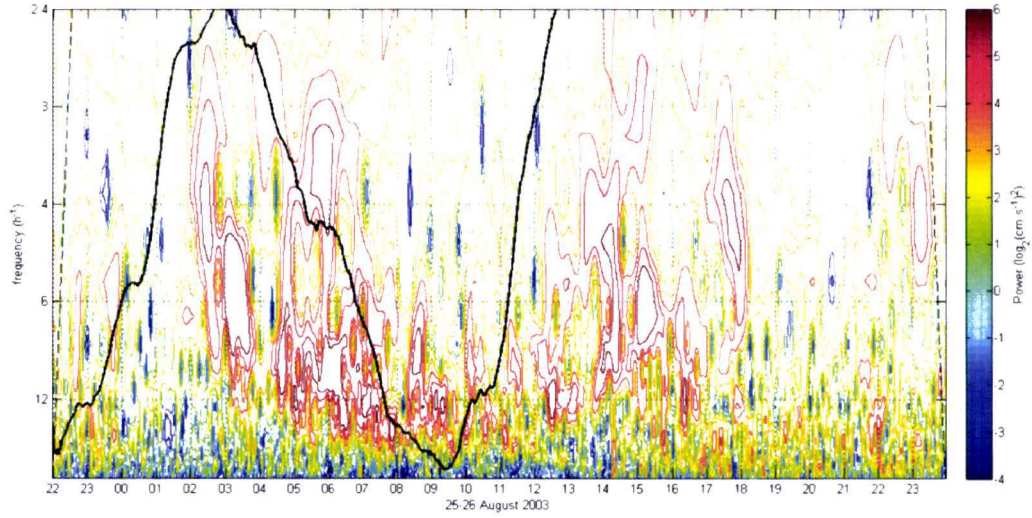


FIG. 28. Reconstructed observed vertical oscillation frequency overlaid on vertical frequency wavelet for 26 August, 2003. Horizontal axis is hours.

DISCUSSION

Vertically oscillating signals in coastal waters 7 km off the New Jersey coast are captured by a VADCP fixed to the sea floor in a 15 m water column. Correlations between the VADCP and the thermistor string suggest that the observed waves are propagating. Because lags are predominantly negative, signals first arrive at the thermistor string and travel parallel to the bathymetric gradient, passing the VADCP, moving towards the coast. The focus of this study was to determine the mechanism responsible for alterations to observed frequencies in the vertical velocity field. An event was defined as having lengths comparable to the tidal period where some maximum in frequency was reached near high tide. The event on 26 August, 2003 was analyzed in detail and the observed change in frequency from the internal wave signal appeared to be Doppler shifted by the barotropic tide. Doppler shifting requires the horizontal current speeds to be comparable in magnitude to the phase speed of the waves present at that time. This also allows for proper flow regimes to exist for the continual propagation of the internal wave in a single direction. The flow regime was subcritical during ebb tide, towards the southeast, and allowed for internal waves to propagate up the bathymetric slope and towards the shore. A transition into the critical regime occurred during flood tide, towards the northwest, and resulted in a stationary wave at the VADCP location. This single event was unique in the fact that horizontal flow during maximum flood tide reached a value that resulted in a critical flow regime; a standing wave was present during the period when high frequencies were observed.

Over 70 events were recorded in the six month time series and are similar to the one previously examined in detail. Wavelet analysis for each event displays an increase

to some maximum frequency before decreasing back to a minimum, and durations of each event are similar to the tidal cycle. For August, wavelet analysis was performed on vertical time series for 56 high tides. Each was examined visually for a change in frequency, specifically looking for a maximum occurring near high tide with a total duration on the order of the tidal cycle. A total of 26 events were realized. Each event varies in the observed range of frequencies which mostly results from stratification. The average of dominant frequencies for 46 complete wavelets over the month of August (± 10 h from each high tide) displays a periodicity equal to the tidal cycle (Fig. 29). The bottom graph shows depth averaged horizontal flow along the flood vector and the corresponding time series of calculated Froude values. A phase speed of 15.5 cm s^{-1} was determined to be the limit of a mode one internal wave from the model based off buoyancy profiles averaged over the month of August. Upon inspection, the month averaged Froude value time series remains subcritical and a critical regime is never reached. A typical wave propagates in the opposite direction of horizontal flow along the flood vector. At the instant when both the horizontal flow and Froude values are zero, the observed frequency is $\omega_{true, August} = 10.0 \text{ h}^{-1}$. This value in conjunction with the Doppler equation results in the black curve on the upper graph (Fig. 29). A t-test comparison indicates the calculated and averaged dominant frequencies over the month of August are not significantly different. Maximums in frequencies occur when Froude values equal zero. Flow before high tide reaches a limit of 3.36 cm s^{-1} and frequencies maintain a relatively constant value of 8.26 h^{-1} . The predominantly shoreward propagating internal wave was being drawn back and forth along the flood direction between each second high tide.

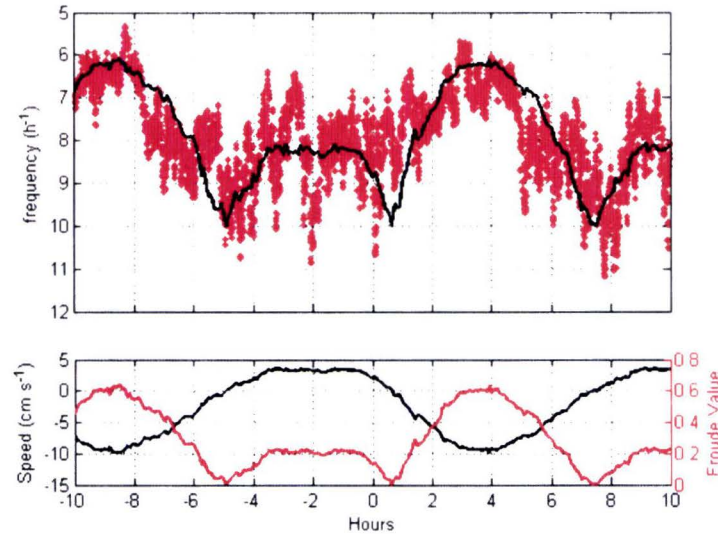


FIG. 29. Vertical oscillation frequencies, top, and horizontal speeds along the flood vector and Froude values, bottom, for the month of August, 2003. Top: dominant frequencies from wavelet analysis averaged over time from maximum tidal amplitude for August, red dots, and computed change in frequency from Eq. (5), solid black line. Bottom: averaged depth averaged horizontal speeds along the flood vector during August, solid black line, and calculated Froude values. Horizontal axis is hours from maximum high tide amplitude.

Table 3 shows the number of observed events with the number of high tides captured by the VADCP. The month of June contains missing data in the VADCP records and therefore is misleading. Low observations for July are due to strong winds that effect horizontal currents; ultimately modifying internal wave structures. The months of May, September, and October contain a low number of observations due to the lack of stratification in the water column. From inspecting all 343 wavelets, a pattern of event/non-event episodes was noticeable. The month of August had comparatively ideal environmental conditions along with consistent VADCP data. Observations were nearly half of the number of tides and are in agreement with events taking place every other high tide.

TABLE. 3. Monthly observed events and number of high tides measured by the VADCP.

	May	June	July	August	September	October
Observations:	11	3	14	26	11	10
Tides:	59	58	58	56	57	55

Vertical mixing is possible in the presence of internal wave at this shallow water location. An instantaneous density profile from hour 13 during the single event analyzed in Section IV suggests relatively large scale overturning near the bottom of the water column (Fig 30). Instability regions here have scales on the order of several metres. A particle excursion can be calculated using half of the internal wave period and a third of the maximum vertical velocity, attributing to a vertical distance of 3.89 metres, or 26% of the height of the water column. This process may lead to vertical sediment redistribution and horizontal transport. Support is found in backscatter imagery, where high particle concentrations are observed near the bottom and middle of the water column.

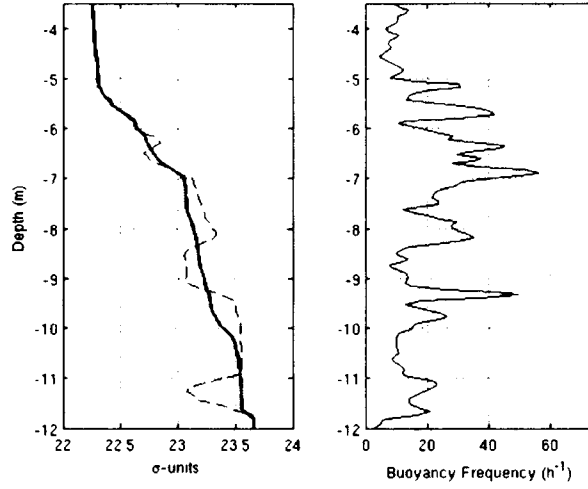


FIG. 30. Density and buoyancy profiles for 13:24, 26 August, 2003. Dashed line, left panel, original measurements and solid line are reordered densities. Densities are in sigma units: $\sigma = \rho_{S,T,p}[\text{kg m}^3] - 1000$.

CONCLUSIONS

Evidence supports propagating internal waves in the direction of the bathymetric gradient towards shore on the New Jersey shelf. Observations show in many cases these waves nearly span the total height of the shallow 15 metre water column. From visual inspection of wavelets produced from over 300 tidal cycles, more than 70 cases contained frequency structures similar to those occurring on 26 August, 2003. Signals have a peak in frequency near high tide and the period of modulation is comparable to the tidal cycle. High variability of environment conditions at this shallow water location, including surface wind forcing and horizontal shear within the water column, play an important role on internal wave propagation. Only when stratification is present can internal waves exist. Events take place when the horizontal currents obtain speeds comparable to the phase speed of the internal wave. As the Froude number approaches a value close to one, a shift in the flow regime occurs and an idealized Doppler shift of the vertical frequency can be observed. Combining the Doppler equation and an internal wave model, the phase speed of an internal wave can be determined from a single location.

Internal waves not only provide an important mechanism for energy transfer from large-scale tides to small-scale vertical mixing, but they are significant for a number of other reasons. Effects can be seen for biological processes when overturning and mixing takes place, transporting nutrients to surface waters enhancing primary production. The ocean is a medium that allows waves to transport heat, energy, and momentum away from distant locations, cascading energy throughout the travel. This displacement of energy from celestial objects to small scale turbulent patches within the ocean is an important area of research and helps to identify basic understandings of the natural world.

REFERENCES

- Apel, J. R., Badiey, M., Chiu, C.-S., Finette, S., Headrick, R. H., Kemp, J., Lynch, J. F., Newhall, A., Orr, M. H., Pasewark, B. H., Tielbuerger, D., Turgut, A., Heydt, K., and Wolf, S., 1997: An overview of the 1995 SWARM shallow-water internal wave acoustic scattering experiment. *IEEE J. Oceanic Eng.*, 22, 465-500.
- Baines, P. G., 1982: On internal tide generation models. *Deep-Sea Res.*, 29, 307-38.
- Beardsley, R. C., and W. C. Boicourt, 1981: On estuarine and continental-shelf circulation in the Middle Atlantic Bight. In B. A. Warren and W. C., editors, *Evolution of Physical Oceanography*, pages 198-233. MIT Press.
- Beardsley, R. C., and C. D. Winant, 1979: On the mean circulation in the Mid-Atlantic Bight, *J. Phys. Oceanogr.*, 9, 612-619.
- Beardsley, R. C., W. C. Boicourt, and D. V. Hansen, 1976: Physical oceanography of the Middle Atlantic Bight. In M. G. Gross, editor, *Middle Atlantic Continental Shelf and the New York Bight*, pages 20-34. Amer. Soc. Limnol. Oceanogr., Special Symposia, 2.
- Bell, T. H., 1975: Topographically generated internal waves in the open sea. *J. Geophys. Res.*, 80, 320-327.
- Bumpus, D. F., 1973: A description of the circulation on the continental shelf of the east coast of the United States. *Prog. Oceanogr.*, 6, 111-157.
- Cairns, J. L., 1974: Internal wave measurements from a midwater float. *J. Geophys. Res.*, 80(3), 299-306.
- Chapman, D. C., and R. C. Beardsley, 1989: On the origin of shelf water in the Middle Atlantic Bight. *J. Phys. Oceanogr.*, 19, 384-391.
- Cushman-Roisin, B., and J.-M. Beckers, 2007: Introduction to Geophysical Fluid Dynamics, Second Edition: Physical and Numerical Aspects, *International Geophysical Series*, Volume 101, 828 pages.
- Egbert, G. B., and R. D. Ray, 2001: Estimates of M2 tidal energy dissipation from TOPEX/POSEIDON altimeter data. *J. Geophys. Res.*, 106, 22475-502.
- Egbert, G. D., and S. Y. Erofeeva, 2002: Efficient inverse modeling of barotropic ocean tides. *J. Atmos Oceanic Technol.*, 19(2), 183-204.
- Egbert, G. B., and R. D. Ray, 2003: Semi-diurnal and diurnal tidal dissipation from TOPEX/POSEIDON altimetry. *Geophys. Res. Letters*, 30(17).

- Espenak, Fred, 2010: Eclipse Predictions. *NASA/Goddard Space Flight Center*, eclipse.gsfc.nasa.gov/eclipse.html.
- Ezer, T., Heman, W. D., Houser, C., and Kjerfve B, 2011: Modeling and observations of high-frequency flow variability and internal waves at a Caribbean reef spawning aggregation site. *Ocean Dyn.* 61, 581-598.
- Gargett, A. E., and J. R. Wells, 2007: Langmuir turbulence in shallow water. Part. 1. Observations. *J. Fluid Mech.*, 576, 27-61.
- Gill, A. E., 1982: *Atmosphere-Ocean Dynamics*. New York: Academic Press, 662 pages.
- Gould, W. J., 1971: Spectral characteristics of some deep current records from the eastern North Atlantic. *Phil. Trans. R. Soc. Lond. A*, 270(1206), 437-50.
- Hallock, Z. R., and R. L Field, 2005: Internal-wave energy fluxes on the New Jersey shelf. *J. Phys. Oceanogr.*, 35, 3-12.
- Hibiya, T., 1986: Generation mechanism of internal waves by tidal flow over a sill. *J. Geophys. Res.*, 91, 7696-708.
- Kohut, J. T., S. M. Glenn, and R. J. Chant, 2004: Seasonal current variability on the New Jersey inner shelf, *J. Geophys. Res.*, 109, C07S07, doi:10.1029/2003JC001963.
- Kunze, E., L. K. Rosenfeld, G. S. Carter, and M. C. Gregg, 2002: Internal waves in Monterey Submarine Canyon. *J. Phys. Oceanogr.*, 32, 1890-913.
- Legg, S., and Adcroft, A., 2003: Internal wave breaking at concave and convex continental slopes. *J. Phys. Oceanogr.*, 33, 2224-2246.
- Legg, S., 2014: Scattering of Low-Mode Internal Waves at Finite Isolated Topography. *J. Phys. Oceanogr.*, 44, 359-383.
- Llewellyn Smith, S. G., and W. R. Young, 2002: Conversion of the barotropic tide. *J. Phys. Oceanogr.*, 32, 1554-66.
- McDougall, T. J., and P. M. Barker, 2011: Getting started with TEOS-10 and the Gibbs Seawater (GSW) Oceanographic Toolbox. *SCOR/IAPSO WG127*, ISBN 978-0-646-55621-5, 28 pages.
- Munk, W. H., and C. Wunsch, 1998: Abyssal recipes II: energetics of tidal and wind mixing. *Deep-Sea Res.*, 45, 1977-2010.
- Pawlowicz, R., B. Beardsley, and S. Lentz, 2002: Classical Tidal Harmonic Analysis Including Error Estimates in MATLAB using T_TIDE. *Computers and Geosciences*, 28, 929-937.

- Phillips, O. M., 1966: *The Dynamics of the Upper Ocean*. Cambridge University Press, 261 pages.
- Richardson, L. F., 1926: Atmospheric Diffusion Shown on a Distance-Neighbour Graph. *Proc. R. Soc. London, Ser. A* 110: 709.
- Smith, S. D., 1988: Coefficients for sea surface wind stress, heat flux, and wind profiles as a function of wind speed and temperature. *J. Geophys. Res.*, 93(C12), 15467-72.
- Tejada-Martinez, A. E., and C. E. Grosch, 2007: Langmuir turbulence in shallow water. Part 2. Large-eddy simulation. *J. Fluid Mech.*, 576, 63-108.
- Thorpe, S. A., 2007: *An Introduction to Ocean Turbulence*. Cambridge University Press. 240 pages.
- Torrence, C., and G. P. Compo, 1998: A Practical Guide to Wavelet Analysis. *Bull. Amer. Meteor. Soc.*, 79, 61-78.
- Yankovski, A. E., and R. W. Garvine, 1998: Subinertial dynamics on the inner New Jersey shelf during the upwelling season. *J. Phys. Oceanogr.*, 28, 2444-2458.

APPENDIX

INTERNAL WAVE MODEL

Based on the linearized, inviscid Navier-Stokes equations and the Boussinesq approximation an equation for the vertical velocity, w , can be obtained:

$$\left(\frac{\partial^2}{\partial t^2} + f^2 \right) \frac{\partial^2 w}{\partial z^2} + \left(\frac{\partial^2}{\partial t^2} + N^2 \right) \nabla_h^2 w = 0, \quad (\text{A.1})$$

where the stability frequency is

$$N^2 = \frac{-g}{\bar{\rho}} \frac{d\bar{\rho}}{dz}, \quad (\text{A.2})$$

and

$$\nabla_h^2 = \frac{\partial^2}{\partial x^2} + \frac{\partial^2}{\partial y^2}. \quad (\text{A.3})$$

A wave solution for w exists with the form:

$$w = W(z) e^{i(k_1 x + k_2 y - \omega t)}. \quad (\text{A.4})$$

The equation for $W(z)$ is then:

$$\frac{d^2 W}{dz^2} + k^2 \left(\frac{N^2 - \omega^2}{\omega^2 - f^2} \right) W = \frac{d^2 W}{dz^2} + k^2 \Gamma^2 W = 0, \quad (\text{A.5})$$

With

$$k^2 = k_1^2 + k_2^2 \quad \& \quad \Gamma^2 = \frac{N^2 - \omega^2}{\omega^2 - f^2}, \quad (\text{A.6})$$

where k is the horizontal wavenumber, ω is the oscillation frequency and f is the coriolis parameter. The boundary conditions at the surface and the bottom are

$$W(0) = W(-H) = 0. \quad (\text{A.7})$$

For a two layer fluid the solutions for W are:

$$W(z) = \begin{cases} W_1 = C_1 \sinh k\Gamma_1 z & -h < z < 0 \\ W_2 = C_2 \sin k\Gamma_2(H + z) & H < z < h \end{cases} \quad (\text{A.8})$$

where

$$\Gamma_1^2 = \frac{N_1^2 - \omega^2}{\omega^2 - f^2} \quad \& \quad \Gamma_2^2 = \frac{N_2^2 - \omega^2}{\omega^2 - f^2}, \quad (\text{A.9})$$

and C_1 and C_2 are arbitrary constants. Imposing continuity of W and W' at transitions between the layers, a system of equations is derived:

$$\begin{pmatrix} \sinh k\Gamma_1 h & \sin k\Gamma_2(H - h) \\ \Gamma_1 \cosh k\Gamma_1 h & -\Gamma_2 \cos k\Gamma_2(H - h) \end{pmatrix} \begin{pmatrix} C_1 \\ C_2 \end{pmatrix} = \begin{pmatrix} 0 \\ 0 \end{pmatrix} \quad (\text{A.10})$$

Requiring the determinant to be zero yields the dispersion relation:

$$0 = \frac{1}{\Gamma_1} \tanh \Gamma_1 k h + \frac{1}{\Gamma_2} \tan \Gamma_2 k (H - h) \quad (\text{A.11})$$

Given a wave frequency ω and providing values for f , h , H and N , wavenumbers k can be found as zeros of this equation and solving numerically one can find eigenvalues representing any number of modes.

- This two-layer numerical model was constructed from a theoretical model derived by Dr. C. E. Grosch – (personal communication).

VITA

WILLIAM DEAN BOLL

wdboll@outlook.com

EDUCATION

- 2015 M.S., Ocean and Earth Sciences, Old Dominion University, Norfolk, VA
 Thesis: *Doppler Shifted Internal Waves in a Shallow Water Region*
 Graduate Certificate in Modeling and Simulation Engineering
- 2009 B.S., Physics, Georgia Institute of Technology, Atlanta, GA

OBJECTIVE: To begin a professional career in the dynamic field of physical oceanography that is challenging, requires critical thinking, and contributes meaningfully to scientific progression.

RESEARCH EXPERIENCE

New York University – Abu Dhabi

- 2013 Center for Global Sea-Level Change
 Assisted with the installation of equipment that collected data associated with glacier production near the Ilulissat Icefjord located southeast of Ilulissat, Greenland. Wrote helicopter deployment procedures for expendable current profilers and X-CTDs.

National Oceanic and Atmospheric Administration

- 2012 NOAA Ship *Okeanos Explorer*
 Aboard Cruise EX1204 to help explore, survey, and map deep-sea canyons and continental margins off the Northeast coast of the United States using multibeam sonar.

Georgia Institute of Technology

- 2008 Chapman Research Lab, Ultracold Atomic Physics and Quantum Optics
 Assisted in the development of optical systems and setups as well as the construction of electronic components and devices. Performed spectroscopy with diode lasers.
- 2007-2008 Georgia Tech Observatory
 Analyzed data taken from intrinsic variable stars and binary star systems through the use of a 16" Schmidt-Cassegrain telescope and CCDOPS cameras. Solved problems that arose with the installation of the telescope and software.

CONFERENCES AND INVITED TALKS

- 2014 Ocean Sciences Meeting, Honolulu, Hawaii
Analysis of VADCP Signals in a Stratified Water Column
- 2013 Center for Sea-Level Change, NYU – Abu Dhabi, Abu Dhabi, UAE
Observations of Wind Generated Internal Waves
- 2012 OCEANS 2012 MTS/IEEE, Hampton Roads, VA